

LLVD: LSTM-based Explicit Motion Modeling in Latent Space for Blind Video Denoising

Loay Rashid^{*1} Siddharth Roheda^{*1} Amit Unde^{*1}

Abstract

Video restoration plays a pivotal role in revitalizing degraded video content by rectifying imperfections caused by various degradations introduced during capturing (sensor noise, motion blur, etc.), saving/sharing (compression, resizing, etc.) and editing. This paper introduces a novel algorithm designed for scenarios where noise is introduced during video capture, aiming to enhance the visual quality of videos by reducing unwanted noise artifacts. We propose the Latent space LSTM Video Denoiser (LLVD), an end-to-end blind denoising model. LLVD uniquely combines spatial and temporal feature extraction, employing Long Short Term Memory (LSTM) within the encoded feature domain. This integration of LSTM layers is crucial for maintaining continuity and minimizing flicker in the restored video. Moreover, processing frames in the encoded feature domain significantly reduces computations, resulting in a very lightweight architecture. LLVD’s blind nature makes it versatile for real, in-the-wild denoising scenarios where prior information about noise characteristics is not available. Experiments reveal that LLVD demonstrates excellent performance for both synthetic and captured noise. Specifically, LLVD surpasses the current State-Of-The-Art (SOTA) in RAW denoising by 0.3dB, while also achieving a 59% reduction in computational complexity.

1. Introduction

Despite significant progress in camera sensor technology, captured images and videos suffer from degradations in perceptual quality due to the presence of noise. The noise in captured images/videos is complex and stochastic in nature due to randomness present in the photon counting process

^{*}Equal contribution ¹Samsung Research Institute, Bangalore. Correspondence to: Loay Rashid <loayrashid1@gmail.com>, Siddharth Roheda <sid.roheda@samsung.com>.

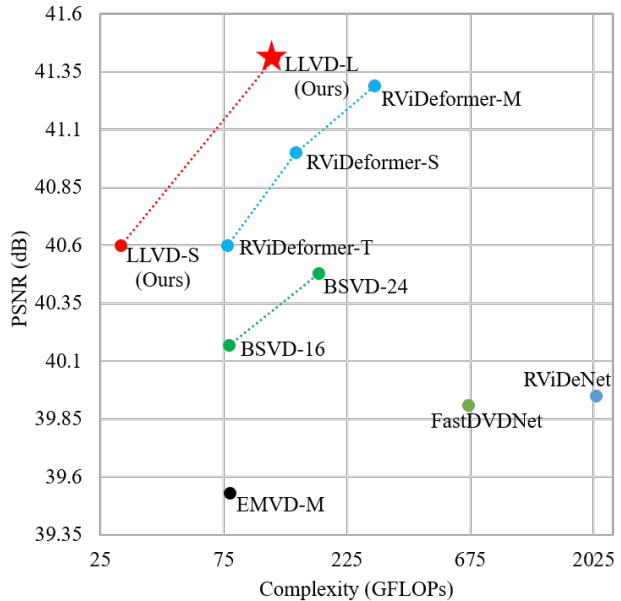


Figure 1: Comparison of PSNR (dB) and computational complexity (GFLOPs) of models on the sRGB CRVD test-set. Compared to existing methods, our models (LLVD-S/L) achieve State-Of-The-Art denoising performance with significantly lower complexity.

and imprecision in the hardware circuitry. This noise causes severe degradation in image quality, especially in unconstrained scenarios such as low-light environments and poor camera sensors. Therefore, denoising, the process of reducing noise artifacts and restoring fine details in images/videos, is an important problem in the field of computer vision.

While the field of image denoising has been extensively explored (Tian et al., 2020), the research community is showing an increasing interest in video denoising. Video denoising differs from image denoising in two key aspects: (1) the temporal correlation between adjacent video frames holds the potential to significantly boost denoising performance and (2) processing the added temporal dimension poses a major computational challenge. Therefore, there is a need for video denoising algorithms which efficiently model the temporal relations present between video frames to boost denoising performance, while simultaneously re-

quiring minimal resources to accommodate computationally constrained systems such as smartphones.

In recent years, a variety of video denoising algorithms have been proposed, ranging from motion-estimation based approaches (Tassano et al., 2019) to emerging learning based approaches (Tassano et al., 2020). From an extensive examination of pre-existing methods, it becomes evident that classical methods based on either frame averaging, spatio-temporal patch based processing (Maggioni et al., 2011), non-local-means filtering (Buades et al., 2005a), or optical flow (Caballero et al., 2016) demand huge processing power, making the extension of these methods to real-time applications extremely challenging.

The advent of Convolutional Neural Networks (CNNs) has marked a significant turning point in this domain. Deep-CNN based algorithms for video denoising have shown significant improvements in performance and are a promising direction of research. CNN-based denoising approaches primarily exploit temporal redundancy either through implicit or explicit motion modeling.

Explicit motion modeling often relies on optical flow and motion estimation and/or compensation techniques (Ren et al., 2017). Despite their efficacy, explicit motion modeling techniques are very computationally intensive, restricting their practical applicability. In this context, a number of algorithms have emerged that capitalize on the strong correlation between neighbouring frames by utilizing multi-stage cascade architectures (Sheth et al., 2021; Yue et al., 2020; Tassano et al., 2020). While this strategy reduces complexity to some extent, it suffers from noticeable reductions in denoising performance. Additionally, these multi-stage methods are still not lightweight enough for denoising on consumer devices.

The inferior performance of implicit motion modeling methods may be attributed to their limited capability in exploiting the temporal correlations between frames. This challenge can be addressed by employing Long Short-Term Memory (LSTM) networks. Known for their excellence in handling sequential data, LSTM networks are ideally suited for modeling the spatio-temporal relationships in video frames, offering a promising solution to enhance video denoising performance.

Contributions: In this paper, we present a novel Latent Space LSTM Video Denoiser (LLVD) dedicated to the vital task of blind video denoising. Our primary contributions include:

- An innovative architecture that seamlessly integrates LSTM layers in the encoded latent space of individual video frames. This approach facilitates the acquisition of temporal relationships between consecutive frames, while also capturing elusive long-term dependencies

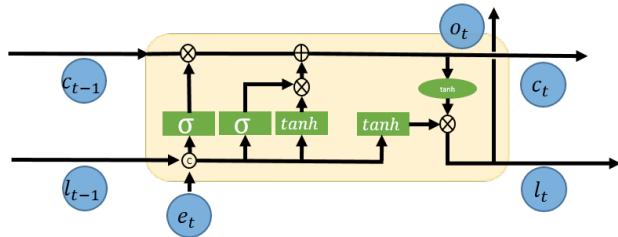


Figure 2: Sequential flow and gating mechanisms in an LSTM layer.

that play a crucial role in the restoration process.

- A light-weight blind denoising approach, which makes video denoising on consumer smartphones (and other embedded devices) a feasible reality. The inclusion of latent LSTMs leads to an astounding reduction in the computations needed for denoising a single frame when compared against SOTA methods.
- We provide a detailed ablation study to highlight and justify the impact of LSTMs in the latent space and demonstrate that they serve as a better alternative to independently using ConvLSTMs or spatial Encoders.
- LLVD demonstrates excellent denoising performance on both synthetic Gaussian noise and real-world captured noise benchmark datasets, achieving SOTA performance without prior information of the noise characteristics, while requiring significantly lower computations.

2. Related Work

2.1. Image Denoising Methods

Denoising is a long-studied field with its roots in traditional signal processing. Since then, numerous methods have been proposed for image/video denoising (Fan et al., 2019; Elad et al., 2023; Tian et al., 2020). Prior to the advent of CNNs in vision tasks, image denoising methods either involved exploiting image priors (Buades et al., 2005b), or using spatial filtering (Benesty et al., 2010; Shin et al., 2005).

With the introduction of CNNs in the vision domain, novel denoising methods demonstrated superior results compared to the previous classical methods (Dong et al., 2014; Zhang et al., 2016; Xie et al., 2012). More recently, attention and transformer-based methods (Anwar & Barnes, 2020; Zamir et al., 2022) have been proposed, achieving excellent performance.

2.2. Video Denoising Methods

Unlike images, videos have a temporal dimension as well. The strong correlation that exists along this temporal axis

in videos can be exploited for enhancing restoration quality. Therefore, work in this domain is focused on modeling spatio-temporal information rather than solely focusing on spatial features. Early work in video denoising explicitly modeled temporal information by utilising block matching (Maggioni et al., 2011) and optical flow (Caballero et al., 2016; Tassano et al., 2019; Ren et al., 2017) to align frames before denoising. However, motion estimation and compensation methods are computationally demanding and are prone to accuracy issues.

To overcome the drawback of high computational complexity associated with spatial domain motion modeling, multi-frame based methods have been proposed (Sheth et al., 2021; Yue et al., 2020; Tassano et al., 2020; Dewil et al., 2021; Claus & van Gemert, 2019), which take multiple consecutive video frames as input and output a single denoised frame. These methods attempt to fuse the information present in consecutive frames, thereby gaining some implicit temporal context for denoising. However, multi-frame based methods suffer from limitations in modeling temporal context since they lack explicit long term temporal modeling. Moreover, each frame needs to be processed multiple times, making these methods computationally inefficient.

Recurrent Neural Networks (RNNs) gained the attention of the research community due to their ability in learning temporal context (Graves et al., 2013; Lei et al., 2018). A number of methods have made use of these recurrent networks for the denoising task (Maggioni et al., 2021; Godard et al., 2018; Sajjadi et al., 2018; Fuoli et al., 2019). While multi-frame methods only have a limited temporal memory, recurrent networks can effectively leverage long-term relationships between past frames and the current frame to enhance restoration quality. More recently, encoder-decoder networks with attention mechanisms (Omray et al., 2020) and transformers (Liang et al., 2022a; Yue et al., 2023) have been introduced, achieving excellent performance at the expense of high computational complexity. Transformers require a large amount of data for training and are computationally inefficient, leading to high training and inference times.

The majority of methods reported in contemporary literature suffer from very high complexities (with GFLOPs in the order of thousands) for processing a single frame. On the contrary, existing lightweight methods (Maggioni et al., 2021; Ehmann et al., 2018) significantly lack denoising performance when compared to their heavier counterparts. Therefore, there is a need to develop lightweight models that can be run with limited computational resources while achieving better denoising quality.

2.3. Long Short-Term Memory

Conventional Recurrent Neural Networks (RNNs) are constrained in their ability to model extensive temporal dependencies, thus limiting the incorporation of a substantial long-term temporal context. To address this limitation, Long Short-Term Memory (LSTM) (Hochreiter & Schmidhuber, 1997) networks were introduced. While initially only being used for Natural Language Processing (NLP) tasks such as machine translation (Sutskever et al., 2014) and language modeling (Sundermeyer et al., 2012), LSTMs have since found utility across a spectrum of vision-related endeavors (Wang et al., 2016; Tatsunami & Taki, 2023).

Additionally, there have been endeavors to enhance the LSTM framework by integrating convolutional kernels, as demonstrated in prior work (Shi et al., 2015). We depict the functioning of an LSTM layer in Figure 2.

3. Problem Formulation

Consider a degraded video sequence, denoted as $\mathbf{Y}_T = \{y_1, y_2, \dots, y_T\}$, comprising T frames. Here, $y_t \in \mathbb{R}^{H \times W \times C}$ is the frame at time t characterized by its height H , width W and channels C . Similarly, we define the corresponding set of clean frames as $\mathbf{X}_T = \{x_1, x_2, \dots, x_T\}$ which undergo degradation to yield the observable frames \mathbf{Y}_T , such that,

$$y_t = f(d(x_t) + n_t). \quad (1)$$

In this context, the function d encapsulates degradations introduced during capture (eg. motion blur, over-exposure, etc), n_t accounts for noise due to the camera sensor, and f encompasses transformations that transpire post-capture (eg. ISP, compression, etc.). Notably, our focus in this work is on a specific scenario where $d(\cdot)$ is an identity operation, leading to the introduction of degradation solely through noise. Moreover, we investigate two distinct scenarios for the function $f(\cdot)$: (i) RAW domain restoration, characterized by $f(\cdot)$ as identity, yielding $y_t = x_t + n_t$, and (ii) RGB domain restoration, wherein $f(\cdot)$ represents the ISP pipeline of the capturing device i.e. $y_t = f(x_t + n_t)$. Our objective is to construct the function $\mathcal{F} : \mathbb{R}^{T \times H \times W \times C} \rightarrow \mathbb{R}^{T \times H \times W \times C}$, which can effectively recover the clean frames denoted as \mathbf{X}_T , such that $\hat{\mathbf{X}}_T = \mathcal{F}(\mathbf{Y}_T) \approx f(\mathbf{X}_T)$ for RGB denoising, and $\hat{\mathbf{X}}_T = \mathcal{F}(\mathbf{Y}_T) \approx \mathbf{X}_T$ for RAW denoising.

4. Proposed Approach

The restoration function \mathcal{F} detailed in Section 3 is constructed through the composition of three distinct functions: a Spatial Encoder (\mathcal{F}_E), a Recurrence Block (\mathcal{F}_L), and a Spatial Decoder (\mathcal{F}_D),

$$\mathcal{F} = \mathcal{F}_E \circ \mathcal{F}_L \circ \mathcal{F}_D. \quad (2)$$

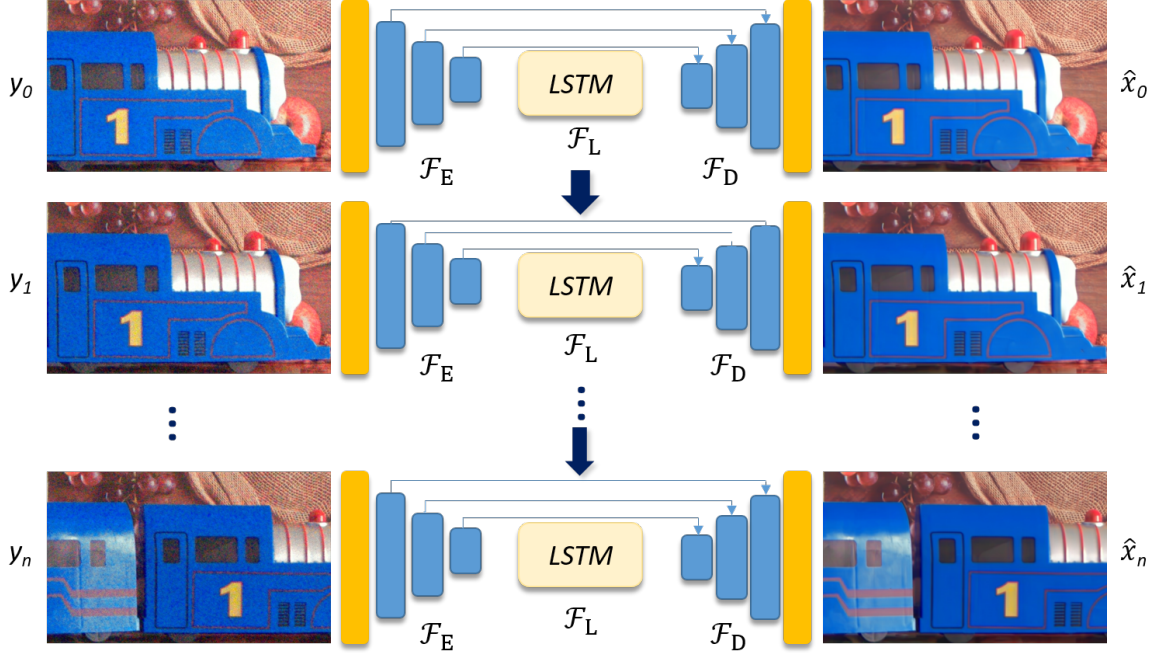


Figure 3: An overview of our proposed method.

4.1. Encoded LSTMs

The Spatial Encoder and Decoder are instrumental in extracting and reconstructing the fine spatial details of video frames. In tandem, an LSTM model, embedded within the encoded latent space, adeptly captures the temporal dynamics. The incorporation of LSTM is crucial in understanding both the immediate and extended temporal relationships between frames, ensuring the production of smooth, flicker-free videos. While past approaches have explored a dual branch approach, segregating the extraction of spatial and temporal features (Chen et al., 2020), our innovation resides in an integrated spatio-temporal approach. Significantly efficient and lightweight, our proposed model is optimally suited for on-device video denoising.

We employ the compositional framework outlined in equation 2 to realize the denoising function \mathcal{F} for enhancing captured videos. Given a noisy video sequence \mathbf{Y}_T , the initial step involves the encoder extracting spatially encoded features for each frame,

$$e_t = \mathcal{F}_E(y_t), \quad \forall t \in \{1, \dots, T\}. \quad (3)$$

Subsequently, a recursive relationship is established among the spatially encoded frames $E_T = \{e_1, \dots, e_T\}$, facilitated by an LSTM model. This LSTM model focuses on capturing the temporal dynamics within E_T , leading to the creation of the ‘spatio-temporal encodings’ $L_T = \{l_1, \dots, l_T\}$,

$$l_t = \mathcal{F}_L(e_t, l_{t-1}, c_{t-1}), \quad \forall t \in \{1, \dots, T\}, \quad (4)$$

where, e_t denotes the spatially encoded frame at time t , l_{t-1} denotes the LSTM output from the preceding time step ($t-1$), and c_{t-1} signifies the LSTM cell state at time ($t-1$). Initialization at $t = 0$ involves setting l_{t-1} and c_{t-1} to 0.

Finally, the ‘spatio-temporal encodings’ L_t undergo decoding through \mathcal{F}_D to reconstruct the pristine video frame as,

$$\hat{x}_t = \sigma(\mathcal{F}_D(l_t)), \quad \forall t \in \{1, \dots, T\}, \quad (5)$$

where σ denotes the sigmoid activation function. A broad overview of our proposed approach can be found in Figure 3.

4.2. Model Architecture

We employ a U-Net inspired architecture for approximating the functions of the Encoder and the Decoder. The input frame at time t undergoes initial processing through the Encoder function, $\mathcal{F}_E : \mathbb{R}^{W \times H \times C} \rightarrow \mathbb{R}^{w \times h \times c}$, structured with three Encoder blocks, each made up of five convolutional layers. Consecutive blocks employ strided convolutions to halve the resolution, resulting in the latent space configuration of $h = H/4$ and $w = W/4$. Subsequently, the recurrent block in the latent space, $\mathcal{F}_L : \mathbb{R}^{w \times h \times c} \rightarrow \mathbb{R}^{w \times h \times c}$, is implemented through a 2-layer LSTM. The choice of Convolutional-LSTM (Shi et al., 2015) architecture is favored over its Fully Connected counterpart due to its convolutional nature, enabling the acquisition of both spatial and temporal information. Finally, the Decoder function, $\mathcal{F}_D : \mathbb{R}^{w \times h \times c} \rightarrow \mathbb{R}^{W \times H \times C}$, is responsible for transform-

ing the spatio-temporally encoded features back into the image space. The Decoder is symmetric in design to the Encoder, with each Encoder block connected to its corresponding Decoder block via a residual connection. The entire architectural arrangement is succinctly depicted in Figure 4.

To further enhance model efficiency, we introduce a Pixel Unshuffle/Shuffle layer before/after the model’s first/last layer, successfully reducing the model complexity by 75%. We refer to the model employing Pixel Shuffle as LLVD-S (Small) and the version without it as LLVD-L (Large). In Section 5, we comprehensively evaluate these models.

4.3. Loss Function Design

The proposed model is guided towards learning the video denoising function, \mathcal{F} , through the minimization of a composite loss function combining L_1 and L_2 distances between the generated denoised video and the Ground Truth. The concurrent use of L_1 and L_2 loss serves to capture both the error magnitude and direction in the model predictions, thereby striking a balance between precision and robustness. While L_2 emphasizes precision and heavily penalizes large errors, it can be very sensitive to outliers. The incorporation of L_1 loss fosters outlier robustness and generates sparse solutions, yielding visually appealing sharper denoised videos. Furthermore, we enhance structural integrity by maximizing the Structural Similarity (SSIM) metric between denoised videos and the Ground Truth. Consequently, the loss function to be minimized is formulated as follows,

$$\min_{\mathcal{F}(\cdot)} \mathcal{L}(\mathbf{Y}_T) = \|\mathcal{F}(\mathbf{Y}_T) - \mathbf{X}_T\|_2^2 + \lambda_1 \|\mathcal{F}(\mathbf{Y}_T) - \mathbf{X}_T\|_1 + \lambda_2 [1 - SSIM(\mathcal{F}(\mathbf{Y}_T), \mathbf{X}_T)], \quad (6)$$

where λ_1 and λ_2 are hyper-parameters governing the influence of individual loss terms. In our experimental setup, we set $\lambda_1 = 0.1$ and $\lambda_2 = 0.01$ to appropriately control these contributions.

5. Experiments

We present two versions of our proposed architecture, LLVD-S (Small) and LLVD-L (Large). To evaluate our method, we use RGB images with synthetic noise and RGB+RAW images with captured noise. Our model’s performance is evaluated against several SOTA video denoising techniques, utilizing Peak Signal-to-Noise Ratio (PSNR) and Structural Similarity Index Measure (SSIM) as evaluation metrics. Finally, we also provide a comparative analysis of the computational complexities associated with these methods, quantified in terms of Giga Floating point Operations (GFLOPs).

The assessment is conducted on scenes sourced from the Captured Raw Video Dataset (CRVD) (Yue et al., 2020) for

real-world sensor noise introduced during capture, DAVIS (Anna et al., 2019) and Set8 (Tassano et al., 2019) for synthetic additive noise.

5.1. Training Details

Real-World Noise: In accordance with (Yue et al., 2020), the initial phase of training uses the Supervised Raw Video Denoising (SRVD) dataset. We employ the Adam optimizer, setting the learning rate at 10^{-4} and batch size to 4. Subsequently, the model is finetuned on scenes 1 through 6 from the CRVD dataset. Evaluation is conducted on scenes 7 to 11 of the same dataset.

Synthetic Noise: Mirroring the data preparation methodology from FastDVDNet (Tassano et al., 2019; 2020), we generate synthetically degraded videos by introducing Additive White Gaussian Noise (AWGN) to videos in the DAVIS training set. Our model’s performance is evaluated on the DAVIS and Set8 testsets, with noise levels of $\sigma \in [10, 20, 30, 40, 50]$.

For both noise models, our network processes 25 frames from each video segment. For the DAVIS dataset, we train on full-resolution (480p) videos, whereas for the CRVD dataset we use randomly cropped 128×128 patches. When processing raw videos, we maintain the CFA Bayer Pattern during spatial cropping as recommended in (Liu et al., 2019). To address the limited 7 frame scope of the CRVD dataset, we extend the training sequence to 25 frames through mirroring. Such an augmentation technique enhances the temporal context for improved learning. Our model is trained using two NVIDIA A100 GPUs.

5.2. Evaluation on Real-world Noise

We conduct a comparative analysis of our method against various video denoising techniques, including FastDVDNet (Tassano et al., 2020), RViDenet (Yue et al., 2020), EMVD¹ (Maggioni et al., 2021), BSVD (Qi et al., 2022), and RViDeformer (Yue et al., 2023). A comprehensive quantitative comparison is showcased in Table 1. We also provide a concise comparison of LLVD-S/L against other methods in Figure 1.

Our experiments reveal that our lighter model, LLVD-S, demonstrates significant superiority over its heavier counterparts in the sRGB domain. Specifically, on the sRGB CRVD testset, LLVD-S achieves performance parity with RViDeformer-T (Yue et al., 2023) ($\sim 2.5\times$ heavier than LLVD-S) and surpasses BSVD-24 with a marginal PSNR improvement of 0.12dB, while concurrently reducing computations by a factor of 6 (See Table 1).

¹Since the code for EMVD has not been released, we use an unofficial implementation: <https://github.com/Baymaxchen/EMVD/>.

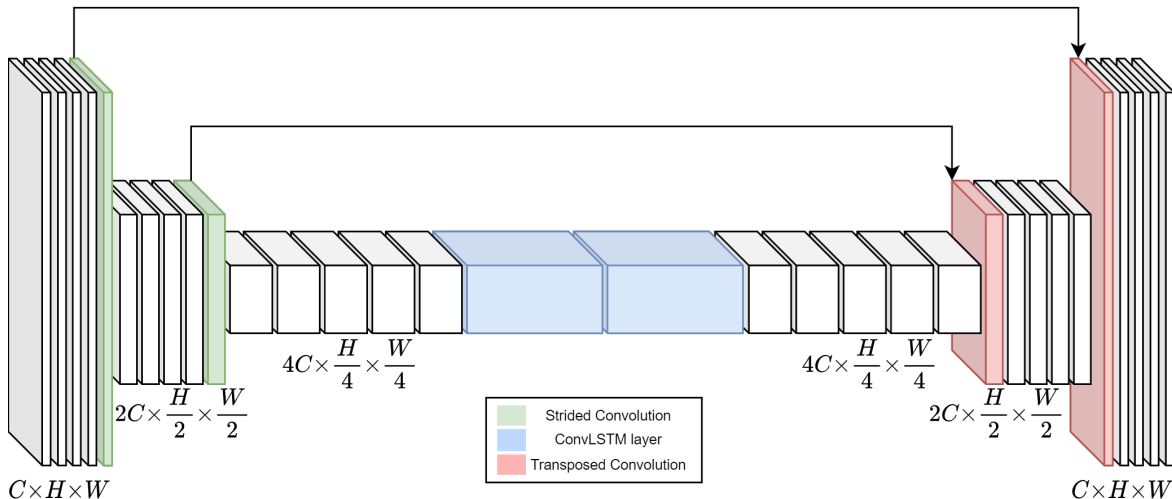
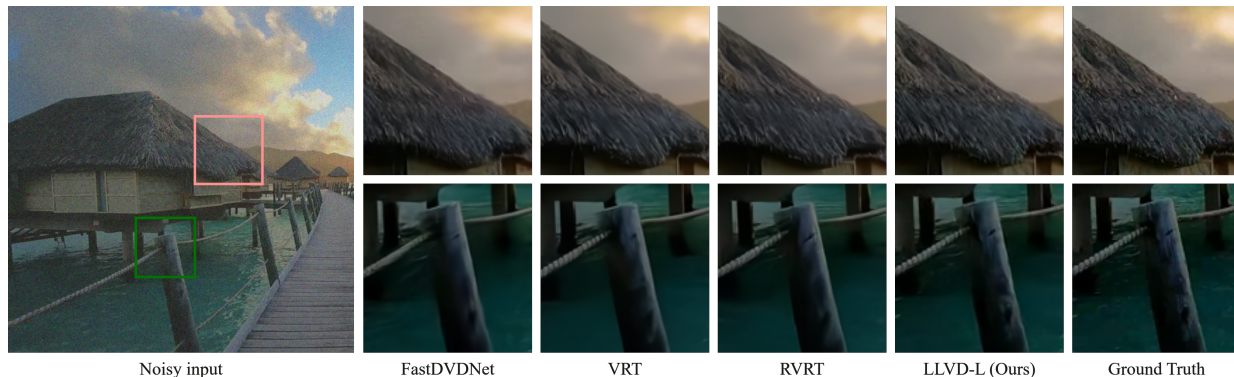
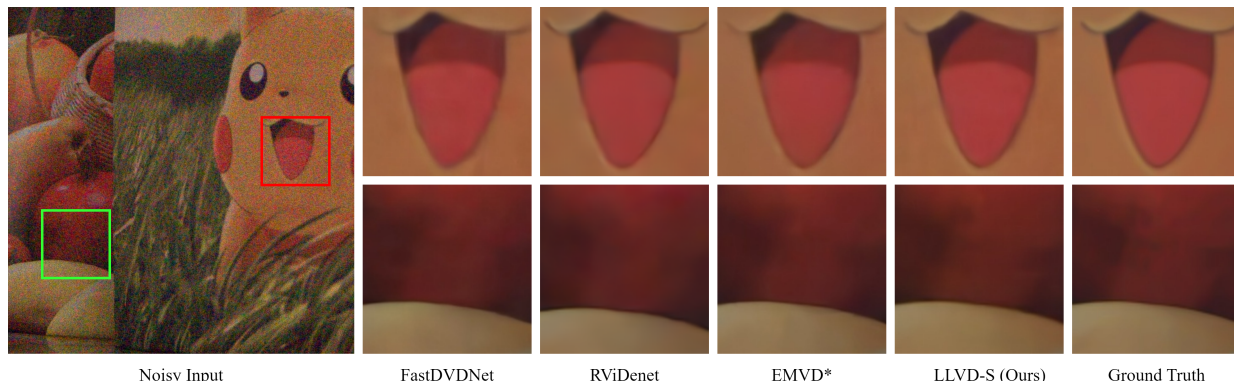


Figure 4: Detailed overview of our model architecture for a single frame. We follow a U-Net style symmetric Encoder-Decoder architecture with skip connections. The encoder and decoder can be broken down into three stages each, with each stage consisting of 5 convolutional layers. The last (first) layer of each stage in the encoder (decoder) performs downsampling (upsampling) using strided convolutions (transposed convolutions). The input video frame and denoised output frame are also connected by a residual connection (not shown).



(a) Set8, $\sigma = 30$



(b) CRVD, ISO 25600

Figure 5: Qualitative comparison on scenes in the CRVD and Set8 testsets. Zoom in for better observation.

For our heavier model, LLVD-L (obtained by removing the pixel shuffle operations), we observe superior denoising prowess over RViDeformer-M ($\sim 2.5\times$ heavier than LLVD-L) by 0.3dB on the raw CRVD testset and 0.1dB on the sRGB CRVD testset. The improved performance of LLVD-S/L over RViDeformer can be attributed to the effectiveness of LSTM in modeling temporal context in latent space while being computationally efficient.

5.3. Evaluation on Synthetic Noise

We also conduct an extensive evaluation of LLVD’s effectiveness on the DAVIS and Set8 datasets, utilizing synthetic AWGN noise. We benchmark LLVD against a variety of blind and non-blind denoising techniques, namely FastDVDNet (Tassano et al., 2020), BP-EVD (Ostrowski et al., 2022), BSVD (Qi et al., 2022), UDVD (Sheth et al., 2021), FloRNN (Li et al., 2022), PaCNet (Vaksman et al., 2021), PTFN (Shibasaki & Ikehara, 2023), VRT (Liang et al., 2022a), RVRT (Liang et al., 2022b), RDRF (Wang et al., 2023), and ReVid (Cao et al., 2022). The comparative analysis is detailed in Table 2.

Our heavier variant, LLVD-L, demonstrates remarkable performance on synthetic noise as well, surpassing all models of similar complexity. In comparison with the current SOTA methods such as VRT, RVRT, RDRF, and ReVid, LLVD-L exhibits a marginal decrease in performance (less than 1 dB) while requiring $10\times$ times fewer computations. Moreover, VRT, RVRT and ReViD are non-blind denoising techniques, which require the noise map as an input. LLVD is noise-blind and does not require any prior information about noise characteristics.

Additionally, we evaluate performance in a cross-dataset setting: evaluating our method on the Set8 testset when trained on the DAVIS dataset. In this setting, LLVD surpasses nearly all denoising techniques except ReViD, indicating the superior generalizability of our method. This cross-dataset performance reinforces LLVD’s capacity for real-world, in-the-wild denoising scenarios.

In addition to our quantitative analysis, we provide visual results in Figure 5. LLVD’s ability to retain high frequency details better than other models can be observed in Figure 5a and in the background areas of Figure 5b.

5.4. Ablation Study

As elaborated in Section 4, our model is composed of three functions (\mathcal{F}_E , \mathcal{F}_L , and \mathcal{F}_D). In our ablation study, we evaluate the impact of these functions on the denoising performance. The training methodology remains consistent with Section 5.1. Table 3 depicts the outcomes of our ablation study.

First, we eliminate all temporal learning elements from the

MODEL	GFLOPs	sRGB		RAW	
		PSNR/SSIM	PSNR/SSIM	PSNR/SSIM	PSNR/SSIM
FastDVDNet-S	22.16	37.43/0.969	42.25/0.980		
EMVD-S	5.38	38.27/0.972	42.63/0.985		
FastDVDNet	664.99	39.91/0.981	44.30/0.989		
EMVD-M	79.52	39.53/0.979	44.05/0.989		
RViDeNet	2079.74	39.95/0.979	43.97/0.987		
BSVD-16	78.76	40.17/0.980	44.10/0.988		
BSVD-24	175.46	<u>40.48/0.982</u>	<u>44.39/0.989</u>		
RViDeformer-T	77.62	40.60/0.981	44.34/0.988		
LLVD-S	29.96	40.60/0.982	43.61/0.993		
EMVD-L	2542.86	–	44.51/0.989		
BP-EVD	131	–	44.42/0.988		
RViDeformer-S	142.6	41.00/0.983	44.65/0.989		
RViDeformer-M	287.34	<u>41.29/0.984</u>	<u>44.89/0.990</u>		
LLVD-L	117.4	41.41/0.984	45.18/0.996		

Table 1: Comparison of our method (LLVD-S/L) against various SOTA video denoising methods. Best results are shown in **bold**, second best are underlined. The results of FastDVDNet-S and FastDVDNet are quoted from (Magioni et al., 2021).

model, rendering it purely spatial. The ConvLSTM layers \mathcal{F}_L are removed, leaving only the encoder-decoder network (\mathcal{F}_E and \mathcal{F}_D). This configuration essentially translates to an image denoising network applied individually to each frame of the video. As anticipated, we observe a substantial drop in the PSNR values, showcasing the indispensability of temporal learning in video data processing. Subsequently, we introduce a single ConvLSTM layer between the encoder-decoder components. Notably there is an improvement over the purely spatial network. Nevertheless, the capacity of a solitary ConvLSTM layer proves inadequate for effective temporal feature extraction. The proposed model with 2 LSTM layers further improves the performance and is optimal for temporal feature extraction.

By completely excluding the encoder-decoder the network is comprised solely of two ConvLSTM layers. We keep the number of channels constant through both layers. Although this arrangement retains spatial learning (due to the use of ConvLSTM layers instead of FC-LSTM layers), the capacity for such learning is markedly constrained, explaining the low PSNR value.

6. Conclusion

In this paper, we proposed a novel approach for Video Restoration, with a focus on denoising in both RAW and RGB domains. The Latent LSTM Video Denoiser (LLVD) demonstrated remarkable performance performance im-

LLVD: LSTM-based Explicit Motion Modeling in Latent Space for Video Denoising

	MODEL	GFLOPS	DAVIS						SET8					
			10	20	30	40	50	AVG	10	20	30	40	50	AVG
NON-BLIND	FastDVDNet	263.20	38.71	35.77	34.04	32.82	31.86	34.64	36.44	33.43	31.68	30.46	29.53	32.31
	BP-EVD	131	39.13	36.04	34.24	32.99	31.97	34.87	37.33	33.95	32.04	30.73	29.73	32.76
	FloRNN	375.25	40.16	37.52	35.89	34.66	33.67	36.38	37.57	34.67	32.97	31.75	30.8	33.55
	PaCNet	117.42	39.97	37.1	35.07	33.57	32.39	35.62	37.06	33.94	32.05	30.7	29.66	32.68
	BSVD-64	486.35	39.81	36.82	35.09	33.86	32.91	35.70	36.74	33.83	32.14	30.97	30.06	32.75
	PTFN	111.45	39.86	37.05	35.41	34.24	33.24	35.96	36.82	33.99	32.36	31.22	30.34	32.95
	VRT	6287.44	<u>40.82</u>	<u>38.15</u>	36.52	35.32	34.36	37.03	<u>37.88</u>	<u>35.02</u>	<u>33.35</u>	32.15	31.22	<u>33.92</u>
	RVRT	515.44	40.57	38.05	<u>36.57</u>	<u>35.47</u>	<u>34.57</u>	<u>37.05</u>	37.53	34.83	33.3	<u>32.21</u>	<u>31.33</u>	33.84
	ReViD	182.8	41.11	38.61	37.1	35.98	35.08	37.58	38.07	35.41	33.87	32.76	31.88	34.4
BLIND	UDVD	OOM	-	-	33.86	32.61	31.63	32.7	-	-	32.01	30.82	29.89	30.91
	RDRF	-	39.54	36.4	34.55	33.23	32.2	35.18	<u>36.67</u>	<u>34.00</u>	<u>32.39</u>	<u>31.23</u>	<u>30.31</u>	<u>32.92</u>
	BSVD-64	486.35	39.68	36.66	34.91	33.68	32.72	35.53	36.54	33.70	32.02	30.85	29.95	32.61
	PTFN	111.45	<u>39.79</u>	<u>36.96</u>	<u>35.31</u>	<u>34.14</u>	<u>33.22</u>	<u>35.88</u>	36.64	33.89	32.28	31.14	30.26	32.84
	LLVD-L	<u>116.5</u>	41.81	37.93	35.8	34.36	33.29	36.64	37.5	35.13	33.55	32.38	31.48	34.01

Table 2: Comparison of our method (LLVD-L) against various SOTA video denoising methods on the DAVIS and Set8 testsets. Best results are shown in **bold**, second best are underlined. The GFLOP values have been calculated for denoising a single frame of 854×480 resolution. The complexity value for ReViD is for a single 256×256 frame as quoted from their paper. At the same resolution, LLVD’s complexity is 18.76 GFLOPs, $10\times$ lighter. The code for ReViD and RDRF is not publicly available.

Table 3: Ablation study, computed on the sRGB CRVD testset.

Pixel Shuffle	×	✓	✓	✓	×
Enc-Dec	×	✓	✓	✓	✓
LSTM (\#)	2	0	1	2	2
GFLOPs	1.50	19.58	24.76	29.96	117.40
PSNR	35.58	38.26	39.96	40.60	41.41
SSIM	0.894	0.968	0.977	0.982	0.984

provements in denoising video frames with both captured and synthetic noise. The implementation of LSTM blocks in the encoded latent space serves as a robust framework for capturing both short-term and long-term temporal relationships without requiring a high computational complexity. Through extensive experimentation, we showcased the superiority of LLVD-L and LLVD-S (a lighter variant of our model for deployment in mobile devices), outperforming heavier models while maintaining reduced computational burden. Our ablation study further underscores the critical importance of each component in our model, emphasizing the significance of temporal modeling for video restoration. Our comprehensive comparison against SOTA denoising methods, as well as the evaluation of both LLVD-L and LLVD-S variants, solidifies the credibility and practicality of the proposed approach. In conclusion, the Latent LSTM Video Denoiser (LLVD) emerges as a promising solution for video denoising on resource constrained devices

such as mobiles, boasting remarkable denoising capabilities, efficiency gains, and a versatile framework for capturing intricate temporal relationships.

References

- Anna, Rohrbach, A., and Schiele, B. Video object segmentation with language referring expressions. In Jawahar, C., Li, H., Mori, G., and Schindler, K. (eds.), *Computer Vision – ACCV 2018*, pp. 123–141, Cham, 2019. Springer International Publishing. ISBN 978-3-030-20870-7.
- Anwar, S. and Barnes, N. Real image denoising with feature attention, 2020.
- Benesty, J., Chen, J., and Huang, Y. Study of the widely linear wiener filter for noise reduction. In *2010 IEEE International Conference on Acoustics, Speech and Signal Processing*, pp. 205–208. IEEE, 2010.
- Buades, A., Coll, B., and Morel, J. Denoising image sequences does not require motion estimation. In *IEEE Conference on Advanced Video and Signal Based Surveillance, 2005.*, pp. 70–74, 2005a. doi: 10.1109/AVSS.2005.1577245.
- Buades, A., Coll, B., and Morel, J.-M. A non-local algorithm for image denoising. In *Proceedings of the 2005 IEEE Computer Society Conference on Computer Vision and Pattern Recognition (CVPR’05) - Volume 2 - Volume 02*, CVPR ’05, pp. 60–65, Washington, DC,

- USA, 2005b. IEEE Computer Society. ISBN 0-7695-2372-2. doi: 10.1109/CVPR.2005.38. URL <http://dx.doi.org/10.1109/CVPR.2005.38>.
- Caballero, J., Ledig, C., Aitken, A. P., Acosta, A., Totz, J., Wang, Z., and Shi, W. Real-time video super-resolution with spatio-temporal networks and motion compensation. CoRR, abs/1611.05250, 2016. URL <http://arxiv.org/abs/1611.05250>.
- Cao, J., Wang, Q., Liang, J., Zhang, Y., Zhang, K., and Van Gool, L. Practical real video denoising with realistic degradation model. arXiv preprint arXiv:2208.11803, 2022.
- Chen, Z., Ramachandra, B., Wu, T., and Vatsavai, R. R. Relational long short-term memory for video action recognition, 2020.
- Claus, M. and van Gemert, J. Videnn: Deep blind video denoising. In Proceedings - 2019 IEEE/CVF Conference on Computer Vision and Pattern Recognition Workshops, CVPRW 2019, IEEE Computer Society Conference on Computer Vision and Pattern Recognition Workshops, pp. 1843–1852, 2019. ISBN 978-1-7281-2507-7. doi: 10.1109/CVPRW.2019.00235. CVPR workshop on NTIRE: New Trends in Image Restoration and Enhancement : NTIRE 2019 ; Conference date: 17-06-2019 Through 17-06-2019.
- Dewil, V., Anger, J., Davy, A., Ehret, T., Arias, P., and Facciolo, G. Self-supervised training for blind multi-frame video denoising, 2021.
- Dong, C., Loy, C. C., He, K., and Tang, X. Learning a deep convolutional network for image super-resolution. In Fleet, D., Pajdla, T., Schiele, B., and Tuytelaars, T. (eds.), Computer Vision – ECCV 2014, pp. 184–199, Cham, 2014. Springer International Publishing.
- Ehmann, J., Chu, L.-C., Tsai, S.-F., and Liang, C.-K. Real-time video denoising on mobile phones. pp. 505–509, 10 2018. doi: 10.1109/ICIP.2018.8451416.
- Elad, M., Kowar, B., and Vaksman, G. Image denoising: The deep learning revolution and beyond – a survey paper –, 2023.
- Fan, L., Zhang, F., Fan, H., and Zhang, C. Brief review of image denoising techniques. Visual Computing for Industry, Biomedicine, and Art, 2(1), July 2019. doi: 10.1186/s42492-019-0016-7. URL <https://doi.org/10.1186/s42492-019-0016-7>.
- Fuoli, D., Gu, S., and Timofte, R. Efficient video super-resolution through recurrent latent space propagation, 2019.
- Godard, C., Matzen, K., and Uyttendaele, M. Deep burst denoising. In Proceedings of the European Conference on Computer Vision (ECCV), September 2018.
- Graves, A., Mohamed, A. R., and Hinton, G. E. Speech recognition with deep recurrent neural networks. CoRR, abs/1303.5778, 2013. URL <http://dblp.uni-trier.de/db/journals/corr/corr1303.html#abs-1303-5778>.
- Hochreiter, S. and Schmidhuber, J. Long short-term memory. Neural Computation, 9(8):1735–1780, 1997.
- Lei, T., Zhang, Y., and Artzi, Y. Training RNNs as fast as CNNs, 2018. URL <https://openreview.net/forum?id=rJBiuunLAW>.
- Li, J., Wu, X., Niu, Z., and Zuo, W. Unidirectional video denoising by mimicking backward recurrent modules with look-ahead forward ones. In Computer Vision – ECCV 2022: 17th European Conference, Tel Aviv, Israel, October 23–27, 2022, Proceedings, Part XVIII, pp. 592–609, Berlin, Heidelberg, 2022. Springer-Verlag. ISBN 978-3-031-19796-3. doi: 10.1007/978-3-031-19797-0_34. URL https://doi.org/10.1007/978-3-031-19797-0_34.
- Liang, J., Cao, J., Fan, Y., Zhang, K., Ranjan, R., Li, Y., Timofte, R., and Gool, L. V. Vrt: A video restoration transformer, 2022a.
- Liang, J., Fan, Y., Xiang, X., Ranjan, R., Ilg, E., Green, S., Cao, J., Zhang, K., Timofte, R., and Van Gool, L. Recurrent video restoration transformer with guided deformable attention. 2022b.
- Liu, J., Wu, C.-H., Wang, Y., Xu, Q., Zhou, Y., Huang, H., Wang, C., Cai, S., Ding, Y., Fan, H., and Wang, J. Learning raw image denoising with bayer pattern unification and bayer preserving augmentation, 2019.
- Maggioni, M., Boracchi, G., Foi, A., and Egiazarian, K. Video denoising using separable 4d nonlocal spatiotemporal transforms. Proceedings of SPIE - The International Society for Optical Engineering, 7870, 02 2011. doi: 10.1117/12.872569.
- Maggioni, M., Huang, Y., Li, C., Xiao, S., Fu, Z., and Song, F. Efficient multi-stage video denoising with recurrent spatio-temporal fusion. In 2021 IEEE/CVF Conference on Computer Vision and Pattern Recognition (CVPR). IEEE, jun 2021. doi: 10.1109/cvpr46437.2021.00347. URL <https://doi.org/10.1109%2Fcvpr46437.2021.00347>.
- Omray, A., Jain, S., Krishnan, U., and Chattopadhyay, P. Exploiting temporal attention features for effective denoising in videos, 2020.

- Ostrowski, P. K., Katsaros, E., Węsierski, D., and Jezierska, A. Bp-evd: Forward block-output propagation for efficient video denoising. *IEEE Transactions on Image Processing*, 31:3809–3824, 2022. doi: 10.1109/TIP.2022.3176210.
- Qi, C., Chen, J., Yang, X., and Chen, Q. Real-time streaming video denoising with bidirectional buffers. In *Proceedings of the 30th ACM International Conference on Multimedia*. ACM, oct 2022. doi: 10.1145/3503161.3547934. URL <https://doi.org/10.1145/3503161.3547934>.
- Ren, Z., Li, J., Liu, S., and Zeng, B. Meshflow video denoising. In *2017 IEEE International Conference on Image Processing (ICIP)*, pp. 2966–2970, 2017. doi: 10.1109/ICIP.2017.8296826.
- Sajjadi, M. S. M., Vemulapalli, R., and Brown, M. Frame-recurrent video super-resolution, 2018.
- Sheth, D. Y., Mohan, S., Vincent, J. L., Manzorro, R., Crozier, P. A., Khapra, M. M., Simoncelli, E. P., and Fernandez-Granda, C. Unsupervised deep video denoising, 2021.
- Shi, X., Chen, Z., Wang, H., Yeung, D., Wong, W., and Woo, W. Convolutional LSTM network: A machine learning approach for precipitation nowcasting. *CoRR*, abs/1506.04214, 2015. URL <http://arxiv.org/abs/1506.04214>.
- Shibasaki, K. and Ikehara, M. Toward high-quality real-time video denoising with pseudo temporal fusion network. *IEEE Access*, 11:81466–81476, 2023. doi: 10.1109/ACCESS.2023.3300028.
- Shin, D.-H., Park, R.-H., Yang, S., and Jung, J.-H. Block-based noise estimation using adaptive gaussian filtering. *IEEE Transactions on Consumer Electronics*, 51(1):218–226, 2005.
- Sundermeyer, M., Schlüter, R., and Ney, H. Lstm neural networks for language modeling. 09 2012. doi: 10.21437/Interspeech.2012-65.
- Sutskever, I., Vinyals, O., and Le, Q. V. Sequence to sequence learning with neural networks. *CoRR*, abs/1409.3215, 2014. URL <http://arxiv.org/abs/1409.3215>.
- Tassano, M., Delon, J., and Veit, T. DVDNET: A fast network for deep video denoising. In *2019 IEEE International Conference on Image Processing (ICIP)*. IEEE, sep 2019. doi: 10.1109/icip.2019.8803136. URL <https://doi.org/10.1109/icip.2019.8803136>.
- Tassano, M., Delon, J., and Veit, T. Fastdvdnet: Towards real-time deep video denoising without flow estimation. In *Proceedings of the IEEE/CVF Conference on Computer Vision and Pattern Recognition (CVPR)*, June 2020.
- Tatsunami, Y. and Taki, M. Sequencer: Deep lstm for image classification, 2023.
- Tian, C., Fei, L., Zheng, W., Xu, Y., Zuo, W., and Lin, C.-W. Deep learning on image denoising: An overview. *Neural Networks*, 131:251–275, 2020. ISSN 0893-6080. doi: <https://doi.org/10.1016/j.neunet.2020.07.025>. URL <https://www.sciencedirect.com/science/article/pii/S0893608020302665>.
- Vaksman, G., Elad, M., and Milanfar, P. Patch craft: Video denoising by deep modeling and patch matching. In *Proceedings of the IEEE/CVF International Conference on Computer Vision (ICCV)*, pp. 2157–2166, October 2021.
- Wang, C., Yang, H., Bartz, C., and Meinel, C. Image captioning with deep bidirectional lstms. *CoRR*, abs/1604.00790, 2016. URL <http://arxiv.org/abs/1604.00790>.
- Wang, Z., Zhang, Y., Zhang, D., and Fu, Y. Recurrent self-supervised video denoising with denser receptive field. *arXiv preprint arXiv:2308.03608*, 2023.
- Xie, J., Xu, L., and Chen, E. Image denoising and inpainting with deep neural networks. *Advances in Neural Information Processing Systems*, 1, 01 2012.
- Yue, H., Cao, C., Liao, L., Chu, R., and Yang, J. Supervised raw video denoising with a benchmark dataset on dynamic scenes. In *IEEE/CVF Conference on Computer Vision and Pattern Recognition (CVPR)*, June 2020.
- Yue, H., Cao, C., Liao, L., and Yang, J. Rvideformer: Efficient raw video denoising transformer with a larger benchmark dataset, 2023.
- Zamir, S. W., Arora, A., Khan, S., Hayat, M., Khan, F. S., and Yang, M.-H. Restormer: Efficient transformer for high-resolution image restoration, 2022.
- Zhang, K., Zuo, W., Chen, Y., Meng, D., and Zhang, L. Beyond a gaussian denoiser: Residual learning of deep CNN for image denoising. *CoRR*, abs/1608.03981, 2016. URL <http://arxiv.org/abs/1608.03981>.